QUASAR - QUAsi-Stationary Absolute Radiance Mission

Eliad Peretz[a], Peter Plavchan[b], Piotr Pachowicz[b], Jamie Tayar[c], Gerard van Belle[d], Greg Aldering[e], Angelle Tanner[f], Justin Albert[g], Dan Huber[h], Leonard Hanssen[i], Brian Alberding[i], Joseph Rice[i], Steven West[a], John Mather[a], Allison Youngblood[a], Tabetha Boyajian[j], Brian Stalder[k], Jonathan Gagné[l], Susana Deustua[i], Kayla Carmical[a], and Andrew Lewis[a]

[a]NASA Goddard Space Flight Center, Greenbelt, MD 20771, USA
[b]George Mason University, Fairfax, Virginia 22030, USA
[c]University of Florida, Gainesville, Florida 32611, USA
[d]Lowell Observatory, Flagstaff, Arizona 86001, USA
[e]Lawrence Berkeley National Laboratory, Berkeley, California 94720, USA
[f]Mississippi State University, Mississippi State, Mississippi 39762, USA
[g]University of Victoria, Victoria, BC, V8W 3P6, Canada
[h]University of Hawaii, Honolulu, HI 96822, USA
[i]National Institute of Standards and Technology, Sensor Science Division, Gaithersburg, MD 20899, USA
[j]Louisiana State University, Baton Rouge, LA 70803, USA
[k]Vera C. Rubin Observatory, Tucson, AZ 85721, USA
[l]University of Montreal, Montreal, Qc, H3T 1J4, Canada

ABSTRACT

This paper describes the scientific and developmental aspects behind the QUAsi-Stationary Absolute Radiance (QUASAR) mission study. The scientific motivation on which the mission is built is established, including the absolute flux calibration of standard and exoplanet host stars, supernova cosmology, and interferometry. Furthermore, we present a science traceability matrix that determines the requirements for the mission through the scientific objectives. Additionally, we provide the mission configuration. This includes the spacecraft structure, its payload, and the component architecture. Finally, we describe how components within the payload provide efficiency and redundancy within the mission.

1. INTRODUCTION

The QUAsi-Stationary Absolute Radiance (QUASAR) mission is a 6U CubeSat mission making significant leaps in reducing, for exoplanets and stars, the uncertainties regarding various properties of these objects. Using QUASAR, uncertainties for stellar flux and Habitable Zone (HZ) location are decreased by factors of >2-10, uncertainties for radii are decreased by factors of >1.4-3, and uncertainties for stellar age and many other properties are lowered. Additionally, QUASAR allows for dark energy parameters' uncertainties to be reduced by a factor of >1.6. These achievements are accomplished by greatly improving the accuracy of visible (VIS) and near-infrared (NIR) absolute zero flux points, which currently are the limiting error budget term in the characterization of stars. The need to reach this goal was identified by the Astrophysics 2020 Decadal Survey as one of its three key scientific themes of "Worlds and Suns in Context." Furthermore, the accuracy of the ratio of the VIS/NIR absolute flux calibration zero point is the limiting error budget term in the Supernovae (SNe) Ia cosmological constraints on dark energy.

QUASAR enables a new "ground truth" for VIS/NIR astrophysics by placing into orbit a National Institute of Standards and Technology (NIST) characterized "artificial star" payload. A 6U Geostationary Transfer Orbit Satellite (GTOSat) mission will be used to place into orbit the payload. We will use a rideshare to a Medium

Further author information: E-mail: eliad.peretz@nasa.gov

Earth Orbit (MEO) / Geosynchronous Transfer Orbit (GTO) to achieve an elliptical orbit around the Earth,[1,2] with an apogee that will be quasi-stationary in the night sky as viewed from the multiple ground telescope stations used by the project.[3–5]

The payload consists of two VIS and two NIR laser diodes, each illuminating an integrating sphere and collimated single mode fibers (SMFs), thereby creating an artificial star for which the photon output and spatial beam profile is known to a required flux precision of <0.5%. By modulating the lasers on and off, recording the emitted flux via onboard photodiodes, monitoring the power and temperature of the lasers, and with 10" precision pointing knowledge from a star-tracker, the knowledge of the absolute flux of the artificial star will be able to be reconstructed. During passes of the spacecraft within the ground-based telescope field of view (FoV) of nearby targets of interest, we will be able to precisely calibrate the absolute flux of these celestial targets to a level never before achieved.

In this paper, we describe the scientific principles fueling the project's development in section 2, discuss the positioning requirements and technical components we will use to reach the project's goals in section 3.1, and present the structure of the spacecraft that will be used in the implementation of QUASAR in section 3.2.

2. SCIENCE

In 1976, VIS/NIR absolute flux calibration accuracy leapt down to ∼1%[6] (Fig. 1) with the mounting of the first CCD on a telescope. Starting in the 1990s, computational advances have advanced relative flux precision from ∼1% to 150 ppm from the ground[7] and 10 ppm from space.[8] In comparison, absolute flux accuracy has stagnated as reliance on atmospheric models lacks a "ground truth" knowledge of the absolute flux rates. However, QUASAR is an orbiting calibration star where the "ground truth" is known to high precision and accuracy to calibrate the flux of celestial observations, opening new scientific vistas.

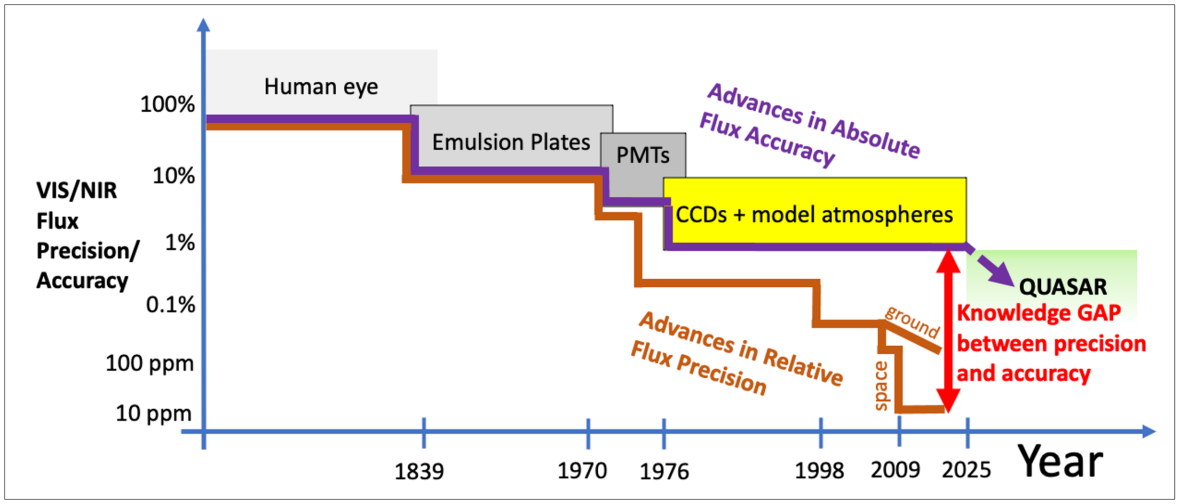

Figure 1. QUASAR will substantially close the knowledge gap between the absolute flux accuracy (purple) and relative flux precision (brown) measurements of celestial objects.

2.1 Absolute Flux Calibration of Standard and Exoplanet Host Stars

Measurements of stellar flux are combined with distance and atmosphere models to estimate a star's radius, temperature, mass, luminosity, and age. These can then be used for stellar science and evolution, galactic archaeology, or in resolved populations of galaxies. In addition, they can be combined with the properties of planets, which are measured relative to their host stars, to infer fundamental irradiance masses, radii, densities, and compositions of exoplanets.

Unfortunately, it does not hold true that the fundamental properties of stars are characterized accurately, and stellar models do not agree on the conversion from observable to fundamental parameters. With QUASAR,

we will be able to directly determine stellar fluxes to <0.5% and radii to <1% (flux α R*2). This also translates into an improvement in the estimated ages of stars by up to a factor of 4 (<10%, Fig. 2). To understand the detailed evolution of our galaxy's chemistry and kinematics, large numbers of stars with precise ages enabled by QUASAR (<20%) are required to improve stellar interior models.[9]

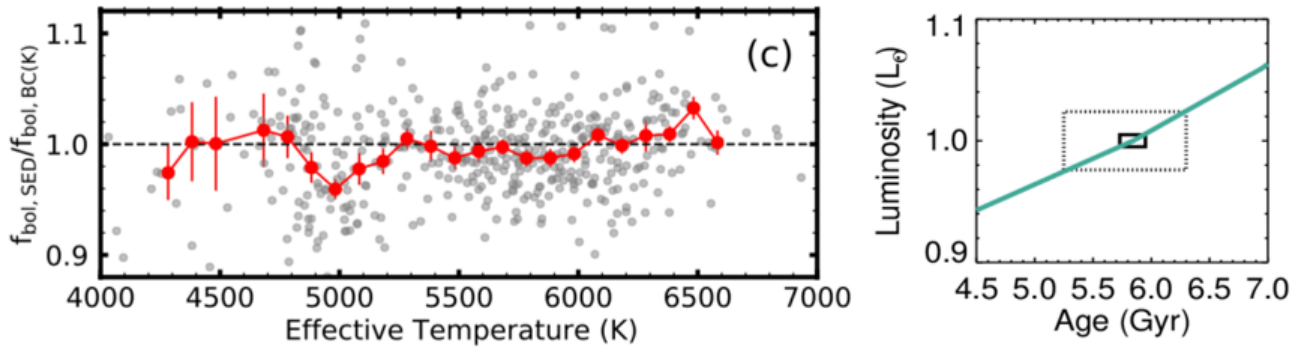

Figure 2. QUASAR will substantially reduce the uncertainties in stellar luminosity, allowing precise stellar age measurements. *Left*: Discrepancies in the estimated bolometric fluxes of exoplanet host stars can vary by 2-4% depending on the method used to estimate the flux (spectral energy distribution fits, SED, versus bolometric corrections, BC, are shown here), which sets a fundamental limit on the uncertainty of the derived luminosity.[9] *Right*: Luminosity (dependent on flux and distance) uncertainties translate to significant (~10%) uncertainties in the implied stellar age.[9] Assuming an optimistic 2.4% luminosity uncertainty (dashed box) at the chosen temperature, and composition (5760 K and solar), the age is 5.775±0.525 Gyrs. With a 0.5% uncertainty (solid box) the age is 5.84±0.11 Gyrs - a factor of 4 smaller.

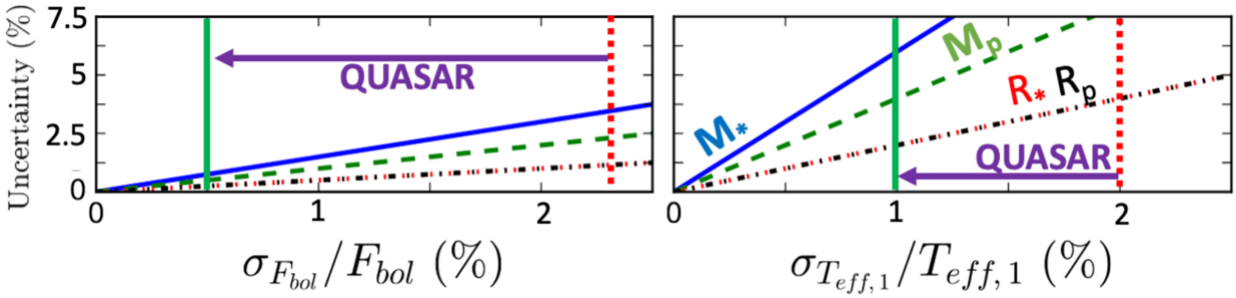

Figure 3. The best achievable model independent accuracy for the planet mass and radius (Mp and Rp, labeled dot-dashed lines) depends directly on the uncertainties of the stellar flux and effective temperature. Current uncertainties (dashed red vertical lines) limit planet mass and radius uncertainties to the 5-7% level. QUASAR will improve the uncertainties in flux and effective temperature to <1% and 1% (green vertical lines), respectively, so that <5% planet masses and <1% planet radii become possible.[10]

With the discovery of thousands of exoplanetary systems, we are transitioning from the discovery era to the characterization era of this field with the James Webb Space Telescope (*JWST*) and the Nancy Grace Roman Space Telescope (*Roman*), which includes the quintessential search for a planet with properties similar to Earth. For exoplanets, uncertainty in stellar flux impacts our ability to accurately determine the HZ location (goes as $\sqrt{\text{luminosity}}$[11–13]), stellar age, and transiting planet radii. With QUASAR, stellar fluxes will be determined to <0.5%, which from Fig. 3 results in planetary radii measured to <2%.[10] QUASAR will make possible robust inferences of more detailed planetary composition.

2.2 Supernova Cosmology

The accelerating expansion of the Universe was discovered using Type Ia SNe, by observing that they were progressively fainter than expected with increasing redshift. Flux calibration accuracy must be uniform with wavelength because differing redshifts result in differing wavelengths for the same rest-frame SN spectral region. The current fundamental flux calibration reference system used for cosmology based on WD atmospheric models[14]

(Fig. 4) has an insufficient accuracy level for Stage-IV cosmology experiments since an error in flux calibration translates to an error 2-3x larger. These experiments require wavelength-relative flux references accurate to <0.5% to compare fluxes in the rest-frame wavelengths between science targets at high and low redshifts.

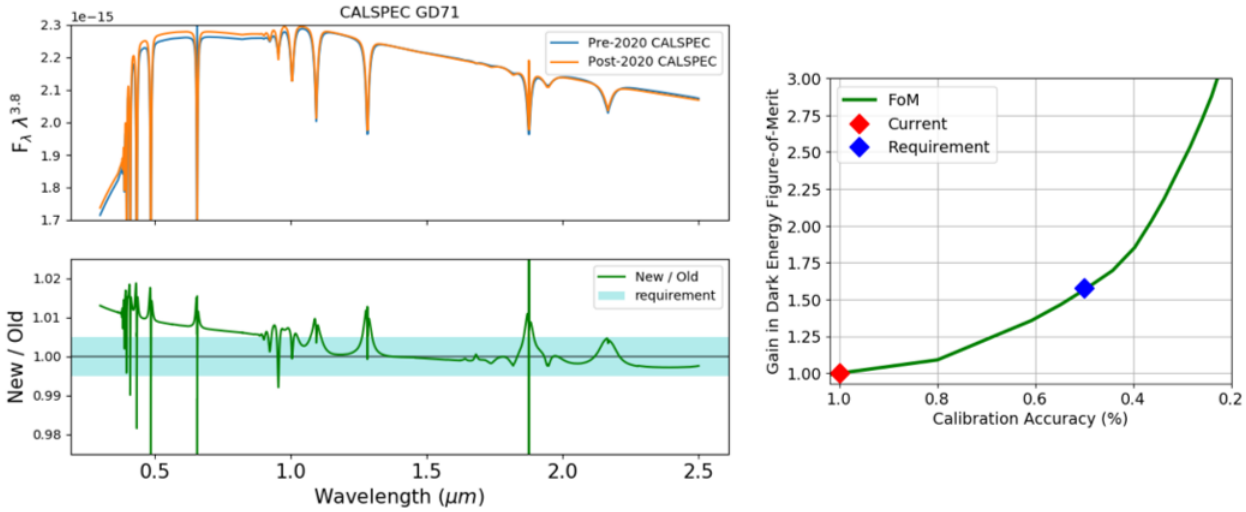

Figure 4. QUASAR will obtain an absolute flux measurement, removing reliance on WD models. *Left* shows the worrisome change in the broadband slope for the flux calibration based on WD atmospheric models.[14] The band shows our ±0.5% requirement. *Right* shows the significant improvement of 1.6x on the relative dark energy figure of merit using SNe Ia with QUASAR and *Roman*. The behavior is close to quadratic, indicating that the figure of merit can improve quickly as the calibration improves. Most of the improvement is along the direction of w_a, which constrains how much dark energy may vary over the history of the universe, of primary interest to cosmologists. Thus, even if QUASAR merely confirms the current calibration but with smaller uncertainties, that will be quite valuable.

2.3 Interferometry

One particularly unique technological capability of QUASAR is to phase ground-based long baseline VIS/NIR interferometers (LBOI). Current United States ground-based LBOI operational facilities are the Center for High Angular Resolution Array (CHARA), and the Navy Precision Optical Interferometer (NPOI) facility. Individual apertures in a LBOI benefit from adaptive optics – both natural and laser guide star (LGS) – but unfortunately, the equivalent of a laser guide star does not exist for LBOIs: the 10-100 micron pathlength variations in the Earth's atmosphere that corrupt signal coherence (at the 10nm level) in such a system are not sampled by an LGS or any similar ground-based system. A QUASAR beacon within the on-sky coherence angle (∼1-2 arcseconds) of a target of interest could be used to phase an LBOI array. As a result, the coherence time could be extended from the atmospheric limit of milliseconds, to many tens of seconds or longer, dramatically improving the sensitivity of these high-angular resolution systems. Imaging young stellar objects with LBOI would provide the necessary angular resolution for probing terrestrial planet formation.[15] QUASAR will demonstrate the feasibility of phasing LBOIs from space.

2.4 Impact and Relevance

QUASAR will revolutionize the accuracy of celestial flux measurements in the VIS/NIR. Because absolute flux calibration of accuracy is so fundamental to observational astrophysics, QUASAR uniquely cuts across all three science themes of the National Academies 2020 Astrophysics Decadal Survey[16] as detailed in section 3.1.1: "Worlds and Suns in Context" through QUASAR's characterization of exoplanet host stars, "Cosmic Ecosystems" through QUASAR's characterization of standard stars, and "New Messengers and New Physics" through QUASAR's enabling constraints on dark energy.

QUASAR will enable *Roman* to meet and potentially exceed its absolute flux calibration requirement in the VIS/NIR (Fig. 4), establish a new model-independent "ground truth" of photon flux rates to calibrate a new set

of standard stars to greater accuracy than is possible otherwise, aid *Roman*'s goal in constraining the Universe's dark energy content, and benefit the Vera C. Rubin Observatory with three laser wavelengths overlapping with its bandpasses (including Y-band). In addition, QUASAR will enhance the science return of *JWST* and the future of NASA's NIR/VIS/UV (ultraviolet) mission, anchoring stellar models and VIS/NIR ancillary measurements and improving our knowledge of the stellar host and exoplanet parameters which will potentially find atmospheric signs of life. Not to mention, the entire Gaia flux catalog could be redone with QUASAR's correction to its flux zero points, as two of our VIS laser wavelengths overlap with the two Gaia bands. Finally, QUASAR offers a technological pathway to phase interferometric arrays on the ground or in space in a way never possible before.

QUASAR can't be done within Earth's atmosphere or with space telescopes alone and requires a space-based calibrated radiator above all of Earth's atmosphere. QUASAR builds upon the payload heritage of the 2U ORCASat launching in 2022, and this will be the second in a succession of additional missions to explore absolute flux calibration across the electromagnetic spectrum.[17] We envision a larger follow-up mission to fly with a higher apogee of 200,000 km for a lower angular drift rate, with more power, λ coverage, and a continuum source for spectroscopy.

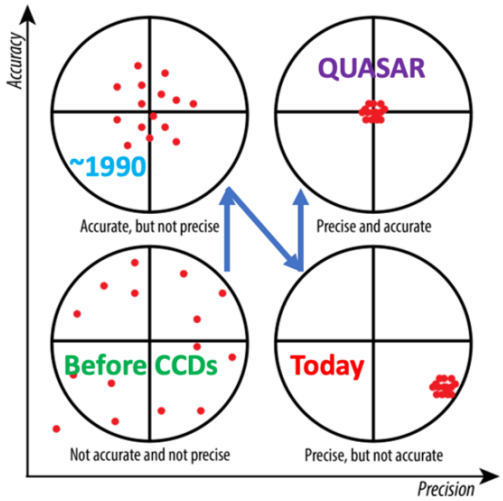

Figure 5. Qualitative precision-accuracy "target plot" showing how QUASAR will enable the next leap in the calibration of flux measurements. We currently can measure VIS/NIR fluxes to great precision but not comparable accuracy (see Fig. 1).

2.5 Science Traceability

QUASAR will advance the precision of the absolute flux calibration of celestial objects over the duration of its one-year primary mission. We present how the scientific requirements of the mission are implemented in Table 1.

3. MISSION IMPLEMENTATION

3.1 Science Implementation Plan

The QUASAR design is driven by the scientific principles presented in section 2.

3.1.1 Mission Orbit

The QUASAR design requires the joint measurement of celestial targets as well as the payload flux of the spacecraft, where it is possible that the spacecraft and the target could both be present within the FoV of the telescope ground station imager. Therefore, a geosynchronous transfer orbit (GTO) was decided to be essential in ensuring this is possible. A GTO allows for long duration data collection and adjustments, as well as the observation of multiple targets as the orbit progresses without the need for the implementation of a propulsion

Table 1. Science traceability matrix for QUASAR.

Science Case	2020 Decadal Themes Addressed	Science Objective	Observable	Mission Requirements
Constrain the habitability of exoplanets through precision determination of their stellar and exoplanet radii and irradiance to <1%	*Worlds and Suns in Context* → Pathways to Habitable Worlds, the top space priority recommendation; Exploring Alien Worlds (2.1.2); The Star-Planet Connection (2.1.2.4);	Absolute Flux Calibration of exoplanet host stars	Simultaneous flux measurement of target star and QUASAR by telescope	<0.5% absolute flux precision; >4x10^4 photoelectrons in exposure times of seconds up to 2 minutes; NIR and/or VIS λs overlapping with Gaia bands; >20 exoplanet host stars, >20 photometric nights
Improve the measured ages of stars and improve the radii determination to <1% to improve our knowledge of stellar evolution and theoretical isochrones across a range of spectral types, ages, rotation and inclinations	*Cosmic Ecosystems* → Stellar and Black Hole Feedback (2.3.2); *Worlds and Suns in Context* → Stellar Demographics (2.1.1)	Absolute Flux Calibration of standard stars	Simultaneous flux measurement of target star and QUASAR by telescope	<0.5% absolute flux precision; >4x10^4 photoelectrons in exposure times of seconds up to 2 minutes; NIR and/or VIS λs with Gaia/Rubin bands; >20 standard stars; >20 photometric nights
Constrain the cosmological parameters for dark energy	*New Messengers and New Physics* → Cosmology and the Dark Sector (2.2.1)	Address systematic errors on dark energy measurements due to flux calibration uncertainties	Flux measurement of QUASAR by telescopes in NIR and Visible wavelengths	<0.5% flux ratio precision between all λ pairings; >4x10^4 photoelectrons in typical exposure time of seconds up to 2 minutes; NIR and VIS λs overlapping Roman and Rubin bands; >20 standard stars; >20 photometric nights
Demonstrate optical interferometry performance of celestial objects	*Worlds and Suns in Context* → Stellar Demographics (2.1.1)	Interferometric Array Phasing Demonstration	Interferometric imaging of QUASAR	>2.5x10^5 $\frac{\text{photons}}{\text{second}}$, V band >6000 km altitude for atmospheric column co-sampling for all array telescopes; coherent light source; NIR and VIS λs; >5 nights, not photometric

system for the spacecraft. Additionally, the orbit ensures that the spacecraft will be quasi-stationary in azimuth at its apogee. Although other orbits could also ensure these measurements could be collected simultaneously, the GTO is ultimately ideal and most efficient for this purpose. Fig. 6 demonstrates the usage of the spacecraft in a geosynchronous transfer orbit.

The feasibility of this orbit has been confirmed by GSFC's CubeSat Launch Initiative (CSLI) representative, and two NASA launch opportunities for the spacecraft have been identified.

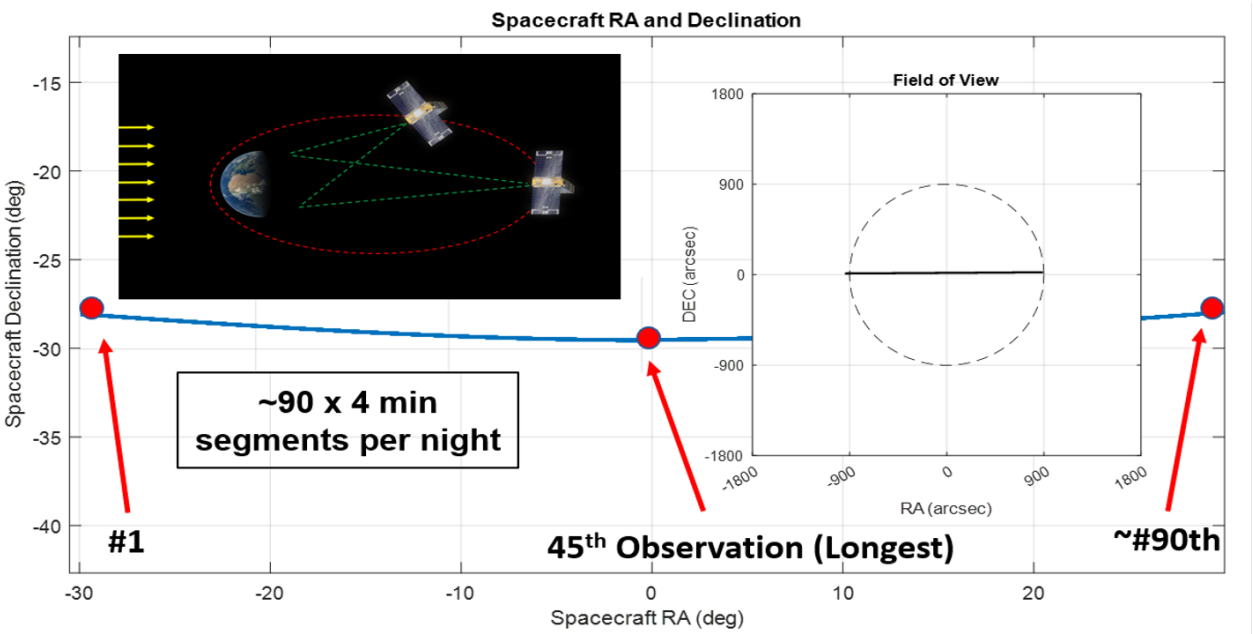

Figure 6. A GTO will create a quasi-stationary artificial star.[18,19] *Left*: The spacecraft at two different points in space in GTO (red), pointing its flux calibrator (green) towards Earth. *Right*: A single imaging sequence duration showing the QUASAR track through the typical ground station 0.5 degree FoV, as viewed from Mauna Kea.[20–22]

3.1.2 Mission Payload

The QUASAR payload is composed of two light sources, including a Fiber Optics Instrument (FOI) and an Integrating Sphere Instrument (ISI). During flux calibration experiments, they will be activated by a satellite bus On-Board Computer (OBC) one at a time. Both sources will take <2U space in the satellite structure and require power levels of <1W, well below the spacecraft payload power of 3W. The design is composed of two light sources, rather than just one, to increase system and measurement reliability and redundancy.

3.1.3 Payload Architecture

The QUASAR payload's top-level block diagram is shown in Fig. 7. Lasers of four different wavelengths—532nm, 775nm, 1064nm, and 1550nm—are fed to the FOI and ISI via single mode fibers (SMFs). For the FOI, these SMFs are connected to a collimator mounted on a post which holds a 45 degree beam sampler. Alternatively, for the ISI, each SMF is connected to the integrating sphere, delivering a uniform but divergent light beam to ground stations. The power state of these lasers will be toggled in a pre-determined sequence, where each laser is given power from anywhere between seconds and minutes. The output from each laser will be measured by the Hamamatsu Silicon and InGaAs photodiodes connected to the beam sampler, where these parts work independently from each other. During the course of a mission, the Control Unit (CU) will be activated as well. These instruments will be connected to the OBC via an RS-422 serial link for commands and telemetry, and interrupt/control (INT/CTRL) lines for diagnostics and other backdoor actions. When the SMFs degrade as expected due to ionizing radiation,[23] the redundancy built into the mission will aid in accounting for this and help prolong the mission's lifetime.

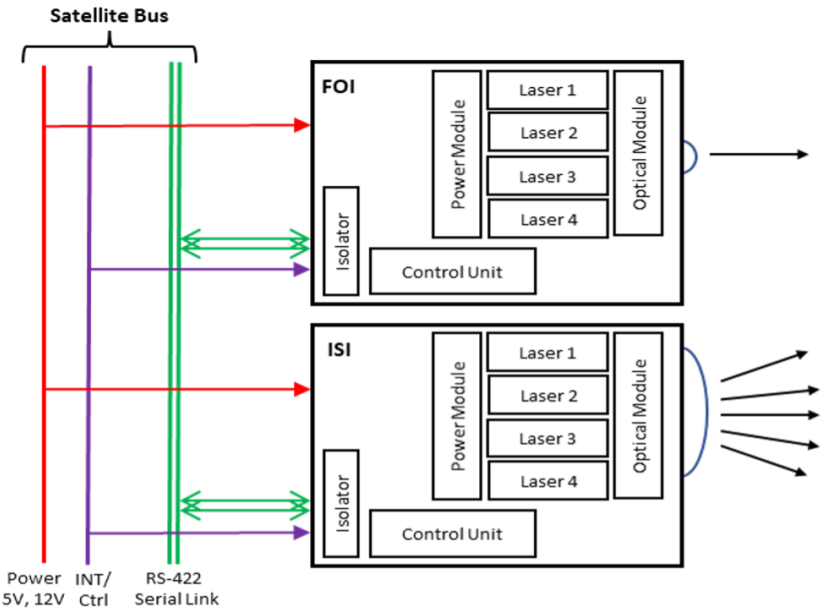

Figure 7. The payload system's architecture is mature with built-in redundancies.

3.1.4 Flight Electronics and Software

Each laser module has a DC/DC power conversion and stabilization unit. Power provided to the lasers and the optical power generated will be recorded over time by voltage, current, temperature, and light intensity sensors. The data produced by this analysis will help assess the impact of the spacecraft's environment on its state, and will aid in analysis of spacecraft degradation for the full lifetime of the mission.

The TI MSP430FR MicroController Unit (MCU) with Ferromagnetic Random Access Memory (FRAM) was selected for QUASAR, as there is no need for high-speed data processing or a large memory requirement. Each CU in the redundant Twin-MCU will have an additional external FRAM storing SP backups, SW config management data, and key system parameters.

3.1.5 NIST Payload Characterization

Critical to the success of QUASAR will be linking the spacecraft FOI and ISI payload illumination sources to NIST standards.

Laboratory measurements can access the far-field of the source beams, but the beam will still be large compared to common beam profiling techniques. Therefore, several techniques for profiling and characterization of the beam must be considered. First, at short propagation distances, a CCD camera will be used to directly profile the beam where the beam reasonably fits in the area defined by the CCD. Second, at larger propagation distances, three options are considered:

1. Raster scan the beam using a small area silicon photodiode;
2. Raster scan the beam using a small area CCD;
3. Illuminate a large target, such as a sheet of polytetrafluoroethylene (PTFE), with the source beam and image the target using the CCD camera equipped with an appropriate lens.

In all of these profiling techniques, the beam profile measurements will be done over a range of distances to determine divergence and stability of the profile with beam propagation. Measurements at short propagation distances can be done using an optical rail system or an automated z-axis stage up to several meters, whereas

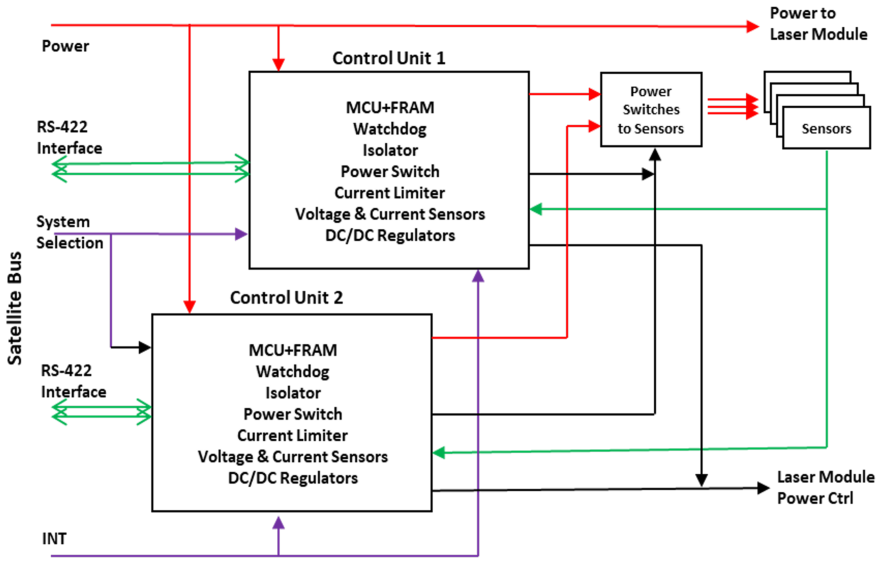

Figure 8. The Twin-MCU architecture allows for redundant SW control. Tasks performed by SW will be triggered by the OBC. Software radiation hardening will be implemented by periodic memory scrubbing. This organization will be supported by FRAM partitioning for in-flight SW updates.

larger propagation distances ranging from 10 meters to around 100 meters can be done utilizing the NIST telescope calibration facility.[24] The various assessment methods will be evaluated, assessed for uncertainty, and compared to theoretical models and the best method will be used to measure the properties of the actual source payload.

3.2 QUASAR Spacecraft

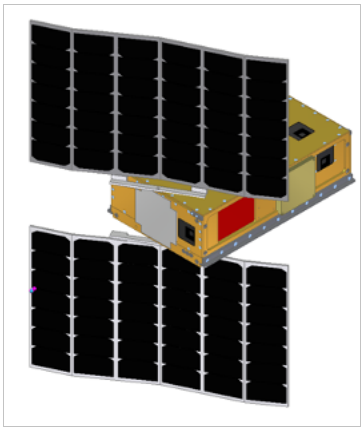

Figure 9. QUASAR spacecraft.

3.2.1 Spacecraft Architecture

The 6U CubeSat includes 3 axis-stabilized pointing control based on sun sensors, a magnetometer, star tracker, IMU, magnetorquers, and three reaction wheels. The telecommunication system will be S-band with patch antennas. The power system includes regulation, switching, lithium-ion batteries, and deployable gimbaled solar panels to minimize solar reflectance to Earth during science operations. The overall size of the spacecraft is 36.6cm x 23.9cm x 11.6cm, conformant to the Planetary Systems Corporation (PSC) 6U canister standard. Initial layouts of the components inside the bus leave nearly 2U of space for the science instrument. Should the

instrument footprint need to be modified, the component locations are easily manipulated in the bus thanks to modular design. Fig. 10 depicts the specific locations of the various components. The design allows for a streamlined build process of the bus and instrument separately so that work can begin immediately.

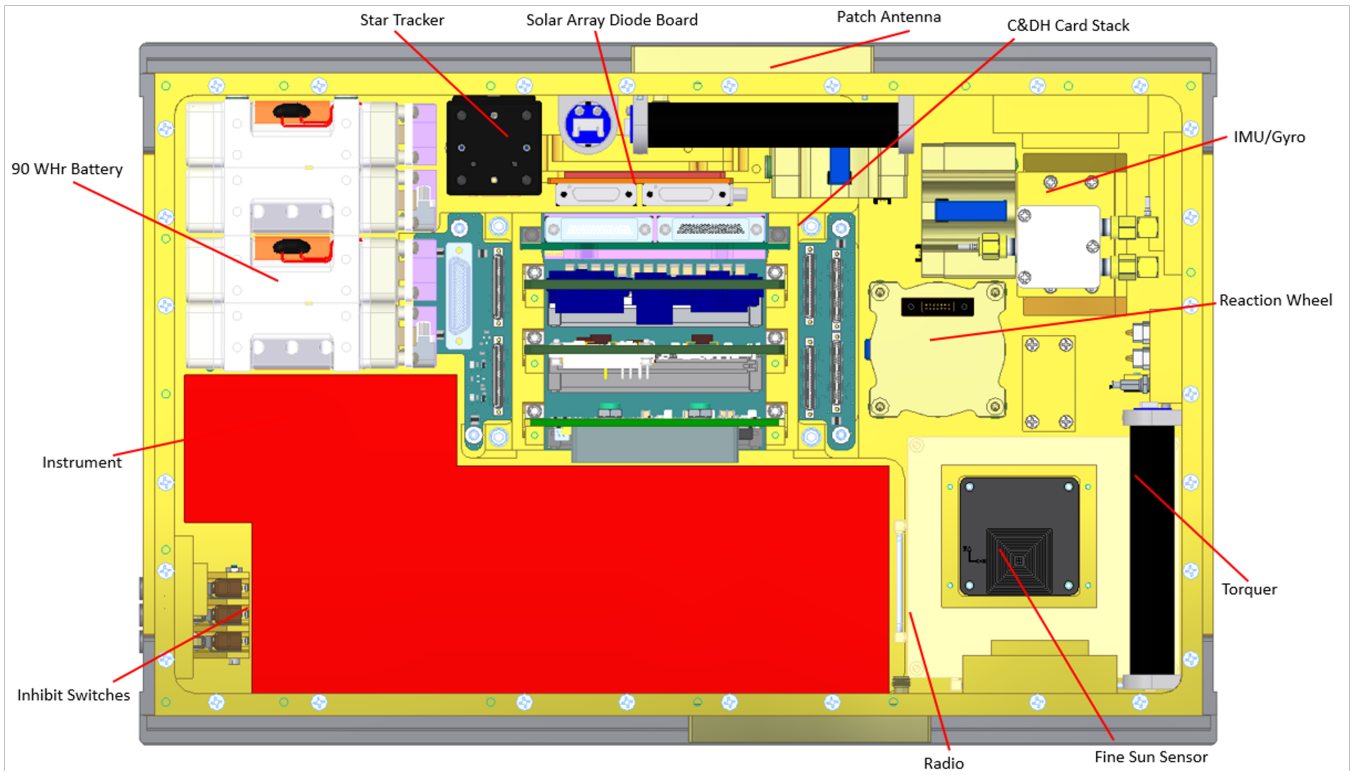

Figure 10. The QUASAR spacecraft layout is modular with ∼2U payload volume.

3.2.2 Structure

The structure is designed and manufactured by NASA GSFC and meets the PSC Canisterized Satellite Dispenser (CSD) Payload Specification 2002367 and the CalPoly CubeSat Design Specification, which states that it can accommodate 12 kg. The primary structure is an aluminum skeleton structure with closeout panels and a lid. The skeletonized baseplate serves as the mechanical interface with the deployer, and contains two tabs to constrain and guide the satellite during launch and ejection. The tabs and load points are separate mechanical pieces. As such, these pieces are easily replaced in the event that they are out of deployer specifications. Closeout panels mounted directly to the skeleton structure can be removed to access component connectors and remove components if needed. Most internal hardware and subassemblies will be mounted directly to the skeletonized baseplate, which will serve as the primary load/thermal path. This internal hardware is mounted from the underside of the structure to ensure bolts can be accessed at all times during integration and testing.

Fine sun sensors and magnetorquers, included on the spacecraft, consist of custom radiation-hardened fine sun sensors and torquer coils that mount directly to the closeout panels, baseplate, and lid, reducing mass and easing integration.

3.2.3 Attitude Determination and Control System

The Attitude Determination and Control System (ADCS) includes coarse and fine sun sensors, a Global Positioning System (GPS), Inertial Measurement Unit (IMU), magnetometer, a star tracker, ferrous core magnetorquer coils, and three 0.010 Nms reaction wheels. The torquers will be used to manage momentum during perigee, when the magnetic field is stronger. The solar arrays will be gimbaled into a low drag configuration during the low perigee to prevent large disturbance momentum buildup. ADCS simulations completed show that while

the momentum build-up during the low perigee exceeds the capability of the reaction wheels, the momentum generated from the torquers can compensate for the build-up and reaction wheels can be used after perigee and throughout apogee accordingly.

3.2.4 Electrical Power Systems

The power system will contain a power management and switching card, four 45 watt-hour (Wh) battery packs (180 Wh total), and two gimbaled deployable solar arrays. During scientific orbits, the satellite will have the instruments and patch antennas pointed toward the nadir direction. During charging orbits and safe mode, the satellite will point the solar arrays directly at the Sun, as the solar panels generate 51 W when in full sun. The EPS will perform all power switching and battery charging while receiving commands and sending telemetry to the OBC.

3.2.5 Thermal Design

The spacecraft utilizes a passive thermal design approach, where the skeletonized structure acts as the main radiator. The thermal design includes a series of coatings, materials, and battery heaters to achieve a balanced system. The heat loads consist of the spacecraft and instrument electronics, direct sun, Earth infrared, and albedo. The power generated by electronics was represented in a multi-node source that couples to the skeletonized structure. A transient analysis demonstrates an operational temperature range of 14-34°C for the science instruments and -5-38°C for the spacecraft throughout the orbit. These temperatures meet the operational range of the FOI, ISI, and spacecraft bus.

3.2.6 Communication Budget, Command and Data Handling, and Flight Software

Spacecraft communication includes semi-real-time S-band for data downlink of I,V,T, data uplink of the schedule of lasers switching on and off, and spacecraft pointing to ground stations. The communication system consists of the Vulcan NSR radio operating in the S-band with patch antennas. The Mission Operations Center (MOC) located at GSFC has a secure remote connection to the Near Earth Network (NEN) ground station to transmit and receive data. Alaska and Wallops Flight Facility stations are also planned for use in the mission. These NEN connections will have a 1 Megabit per second (Mbps) real-time link.

The Processor Board is equipped with a Microsemi RTG4 Field Programmable Gate Array (FPGA) that is designed to withstand harsh radiation environments. It contains a soft-core processor and the Flight SW (FSW) code for the QUASAR Avionics, and allows the integration of Command and Data Handling (C&DH), an attitude control system (ACS), front end communications, and housekeeping interface functionality into a single device.

The Flash device stores all science data captured, spacecraft housekeeping data, and copies of the FSW code. It can store a large enough amount of data to store this information over multiple orbits. The processor board carries I2C and SPI interfaces for communications with other systems, with an adapter board that contains the analog circuitry to convert temperature, voltage, and current data collected from multiple points to a digital format that can be processed, stored, and downlinked.

REFERENCES

[1] Peretz, E., Hamilton, C., Mather, J., D'Amico, S., Michaels, A., Pritchett, R., Yu, W., and Wizinowich, P., "Astrostationary orbits for hybrid space and ground-based observatories," *Journal of Astronomical Telescopes, Instruments, and Systems* **8**(1) (2022).

[2] Koenig, A. W., D'Amico, S., Peretz, E., Yu, W., Hur-Diaz, S., and Mather, J., "Optimal spacecraft orbit design for inertial alignment with ground telescope," IEEE Aerospace Conference (March 2021).

[3] Peretz, E., Ugolnikov, O. S., and Postylyakov, O. V., "Orbiting configurable artificial star (orcas) for visible adaptive optics from the ground," *Astronomy & Astrophysics* **51**, 385–393 (Aug. 2006).

[4] Peretz, E., Hamilton, C., Mather, J., Pabarcius, L., Hall, K., Michaels, A., Pritchett, R., Yu, W., Wizinowich, P., and Golliher, E., "Orcas–orbiting configurable artificial star mission architecture," *UV/Optical/IR Space Telescopes and Instruments: Innovative Technologies and Concepts X.* **11819** (2021).

[5] Peretz, E., Mather, J., Slonaker, R., O'Meara, J., Seager, S., Campbell, R., Hoerbelt, T., and Kain, I., "Orbiting configurable artificial star (orcas) for visible adaptive optics from the ground," in [*Bulletin of the American Astronomical Society*], *APC White Papers, no. 284* **51**(7), Astro2020: Decadal Survey on Astronomy and Astrophysics (2019).

[6] Bohlin, R., Hubeny, I., and Rauch, T., "New grids of pure-hydrogen white dwarf nlte model atmospheres and the hst/stis flux calibration," *The Astronomical Journal* **160** (June 2020).

[7] Stefansson, G., Mahadevan, S., Hebb, L., Wisniewski, J., Huehnerhoff, J., Morris, B., Halverson, Ming Zhao, S., Wright, J., O'rourke, J., Knutson, H., Hawley, S., Kanodia, S., Li, Y., Hagen, L., Liu, L., Beatty, T., Bender, C., Robertson, P., Dembicky, J., Gray, C., Ketzeback, W., McMillan, R., and Rudyk, T., "Toward space-like photometric precision from the ground with beam-shaping diffusers," *The Astrophysical Journal* **848** (Oct. 2017).

[8] Borucki, W. J., Koch, D., Basri, G., Batalha, N., Brown, T., Caldwell, D., Caldwell, J., Christensen-Dalsgaard, J., Cochran, W. D., Devore, E., Dunham, E. W., Dupree, A. K., G. I. T. N., Geary, J. C., Gilliland, R., Gould, A., Howel, S. B., Jenkins, L. M., Kondo, Y., Latham, D. W., Marcy, G. W., Meibom, S., Kjeldsen, H., Lissauer, J. J., Monet, D. G., Morrison, D., Sasselov, D., Tarter, J., Boss, A., Brownlee, D., Owen, T., Buzasi, D., Charbonneau, D., Doyle, L., Fortney, J., Ford, E. B., Holman, M. J., Seager, S., Steffen, J. S., Welsh, W. F., Rowe, J., Anderson, H., Buchhave, L., Ciardi, D., Walkowicz, L., Sherry, W., Horch, E., Isaacson, H., Everett, M. E., Fischer, D., Torres, G., Johnson, J. A., Endl, M., Macqueen, P., Bryson, S. T., Dotson, J., Haas, M., Kolodziejczak, J., Van Cleve, J., Chandrasekaran, H., Twickene, J. D., Quintana, L. V., Clarke, B. D., Allen, C., Li, J., Wu, H., Tenenbaume, P., Verner, K., Bruhweiler, F., Barnes, J., and Prsa, A., "Kepler planet-detection mission: Introduction and first results," *Science* **327** (Jan. 2010).

[9] Tayar, J., Claytor, Z., Huber, D., and van Saders, J., "A guide to realistic uncertainties on fundamental properties of solar-type exoplanet host stars," *The Astrophysical Journal* **927** (March 2022).

[10] Stevens, D., Gaudi, B., and Stassun, K., "Measuring model-independent masses and radii of single-lined eclipsing binaries: Analytic precision estimates," *The Astrophysical Journal* **862** (July 2018).

[11] Kasting, J., Whitmire, D., and Reynolds, R., "Habitable zones around main sequence stars," *Icarus* **101** (Jan. 1993).

[12] Kane, S., "Habitable zone dependence on stellar parameter uncertainties," *The Astrophysical Journal* **782** (Feb. 2014).

[13] Kane, S., Barcla, T., and Gelino, D., "A potential super-venus in the kepler-69 system," *The Astrophysical Journal Letters* **770** (May 2013).

[14] Bohlin, R., Gordon, K., and Tremblay, P., "Techniques and review of absolute flux calibration from the ultraviolet to the mid-infrared," *The Astronomical Society of the Pacific* **126** (2014).

[15] Monnier, J., Rau, G., Bermudez, J., Ragland, S., Akeson, R., Duchene, G., Belle, G., Norris, R., Gordon, K., Defrère, D., Kluska, J., Ridgway, S., Le Bouquin, J., Anugu, N., Scott, N., Kane, S., Richardson, N., Regaly, Z., Zhu, Z., Vasisht, G., Stassun, K., Andrews, S., Lacour, S., Weigelt, G., Turner, N., Adams, F., Gies, D., Calvet, N., Espaillat, C., Millan-Gabet, R., Gardner, T., Packham, C., Gai, M., Kral, Q., Berger, J., Linz, H., Klarmann, L., Bate, M., Bae, J., Lopez, R., Garufi, A., Baron, F., Kama, M., Wilner, D., Hartmann, L., Kishimoto, M., Olofsson, J., McClure, M., Haniff, C., Hoenig, S., Line, M., Petrov, R., Smith, M., Brummelaar, T., De Furio, M., Koutoulaki, M., Rinehart, S., Leisawitz, D., Danchi, W., Huber, D., Zhang, K., Pope, B., Ireland, M., Kraus, S., Isella, A., Setterholm, B., and White, R., "Imaging the key stages of planet formation," *Bulletin of the American Astronomical Society* **51** (May 2019).

[16] "Decadal survey on astronomy and astrophysics 2020 (astro2020)." www.nationalacademies.org/our-work/decadal-survey-on-astronomy-and-astrophysics-2020-astro2020.

[17] "Orcasat." https://www.orcasat.ca/.

[18] Peretz, E., Mather, J., Slonaker, R., O'Meara, J., Seager, S., Campbell, R., Hoerbelt, T., and Kain, I., "Orbiting Configurable Artificial Star (ORCAS) for Visible Adaptive Optics from the Ground," in [*Bulletin of the American Astronomical Society*], **51**, 284 (Sept. 2019).

[19] Peretz, E., McCormick, K., Moehring, E., Hamilton, C., Mather, J., Hall, K., Hyland, D., Freeman, A., Russin, T., Nash, J., and Robie, D., "Orbiting configurable artificial star multi-wavelength laser payload," *Astronomical Optics: Design, Manufacture, and Test of Space and Ground Systems III* **11820** (2021).

[20] Peretz, E., Hall, K., Mather, J. C., Shaklan, S., and Hildebrandt, S., "Exoplanet imaging performance envelopes for starshade based missions," *Journal of Astronomical Telescopes, Instruments, and Systems* **7** (2020).

[21] Peretz, E., Mather, J. C., Hall, K., Canzoniero, C. M., Pabarciusa, L., Gilchrist, K., Lieber-Kotza, M., Slonaker, R., Yu, W. H., Hughes, S., Hur-Diaza, S., Koenigb, A., and D'Amico, S., "Exoplanet imaging scheduling optimization for an orbiting starshade working with extremely large telescopes," *Journal of Astronomical Telescopes, Instruments, and Systems* **7**(1) (2020).

[22] Peretz, E., Mather, J., Parbarcius, L., and *et al.*, "Mapping the observable sky for a remote occulter working with ground-based telescopes," *Journal of Astronomical Telescopes, Instruments, and Systems* **7**(1) (2021).

[23] Girard, S., Morana, A., Ladaci, A., Robin, T., Mescia, L., Bonnefois, J., Boutillier, M., Mekki, J., Paveau, A., Cadier, B., Marin, E., Ouerdane, Y., and Boukenter, A., "Recent advances in radiation-hardened fiber-based technologies for space applications," *Journal of Optics* **20** (Aug. 2018).

[24] "Telescope Calibration Facility (TCF)." https://www.nist.gov/laboratories/tools-instruments/telescope-calibration-facility-tcf.